Theoretical Model and Analysis on the Locally Concentrated Current and Heat During Electromagnetic Propulsion

KEREN DAI [ID], (Member, IEEE), YUXIN YANG, QIANG YIN, AND HE ZHANG
ZNDY of Ministerial Key Laboratory, School of Mechanical Engineering, Nanjing University of Science and Technology, Nanjing 210094, China

Corresponding authors: Keren Dai (dkr@njust.edu.cn) and He Zhang (hezhangz@njust.edu.cn)

ABSTRACT Electromagnetic propulsion technology has important applications in military equipment such as electromagnetic rail guns. The extremely harsh multiphysics environment during electromagnetic propulsion is the key problem that now restricts its practical application. Most previous modeling studies have neglected or set overidealized approximations for the coupling effects between different physics fields, resulting in large deviations between simulated and actual results. In this paper, the multi-field coupling dynamic model of the electromagnetic propulsion process is established. Based on this model, the dynamic changes of the armature's speed, current distribution and temperature distribution during the electromagnetic propulsion process are effectively simulated, and some characteristics of these distributions are different from the previous uncoupled model. Furthermore, the physical mechanism behind these special distribution features is revealed, and the significance of the nonideal factors such as the piezoresistive effect of contact resistance and friction effect of the contact interface on the electromagnetic propulsion are analyzed. Therefore, a feasible path for the simplification of the multiphysics model and the relief of the extreme environment is revealed, which will greatly promote the practical application of electromagnetic propulsion technology.

INDEX TERMS Current distribution, current skin effect, dynamic multi-field coupling model, electromagnetic propulsion, temperature distribution.

I. INTRODUCTION

In recent years, electromagnetic propulsion technology has made many breakthroughs in the fields of aircraft launch [1], [2] and advanced artillery [3]–[6]. With the help of electromagnetic forces generated by strong magnetic fields and large currents, electromagnetic propulsion technology can achieve a target speed of 2000 m/s or higher in a few milliseconds [7], easily surpassing the speed limit of traditional chemical propulsion technology. During the electromagnetic propulsion process, the dynamically changing environment including extremely strong dynamic shock, a strong electromagnetic field and high temperature poses a serious threat to the reliability of the electronic system in the propulsion load and the life of the propulsion system [8].

The associate editor coordinating the review of this manuscript and approving it for publication was Wen-Sheng Zhao [ID].

Due to the difficulty of highly dynamic and accurate measurement of multiphysics extreme environmental parameters, modeling and simulation are the main ways of analyzing the extreme environment during electromagnetic propulsion and optimizing the design of electromagnetic propulsion systems [9], [10].

Early studies on electromagnetic propulsion modeling mostly used equivalent circuit models and involved only a single physical quantity such as temperature or magnetic field [11], [12]. Although these equivalent circuit models are easy to calculate, there are large deviations compared with the actual physical field during the electromagnetic propulsion process. In addition, the parameters in these models depend on accurate experimental measurements, which are often difficult to accomplish. Compared with the equivalent circuit model, physical field modeling can reflect the dynamics of the propulsion process and can achieve more accurate

K. Dai *et al.*: Theoretical Model and Analysis on the Locally Concentrated Current and Heat During Electromagnetic Propulsion

IEEE*Access*

simulation results, so it has been further developed in recent years [13]–[15]. For the single physics field, Ghassemi *et al.* realized the simulation of the magnetic field distribution [16], and Bayati *et al.* realized the simulation of the temperature field distribution [17]. Furthermore, by associating the multiphysics models, researchers have discovered some important physical effects during the electromagnetic propulsion process. For example, Yin *et al.* studied the velocity skin effect on the electromagnetic field [18], Xia *et al.* studied the effect of contact resistance under pressure on the electromagnetic field [19], and Gong studied the friction effect on the electromagnetic propulsion process [20]. These efforts have promoted the understanding of the extreme environment of the electromagnetic propulsion process and its formation mechanism. They also show that modeling of coupled multiphysics fields is the main way to reveal the extreme environment during the electromagnetic propulsion process.

However, although some associations between physical fields are introduced in these multiphysics modeling methods, they leave something to be desired for practical applications. Some only consider the effect of one physics field on another, while the reverse impact is ignored; others need a large number of quasistatic approximations. For example, Yin *et al.* [18] studied the influence of velocity on the electromagnetic field, which is the velocity skin effect. However, the influence of electromagnetic force on velocity is ignored, and a known dynamic change in velocity is assumed. Therefore, these studies are not really multiphysics coupling models in the true sense. In fact, the importance of research on the coupling effect between multiphysics fields has been revealed by many studies in other fields. It is usually the fatal factor that accelerates the reaction and causes the extreme environment in a very short time [21]–[23]. To ensure the reliability of electromagnetic propulsion, it is necessary to study the coupling relationship between physical fields and establish a multiphysics coupling model of electromagnetic propulsion process.

In this paper, the coupling relationship between the mechanical and electromagnetic fields during electromagnetic propulsion is studied, and a multifield physics model including the electromagnetic field, mechanical field and thermal field is carried out. Based on the proposed model, dynamic simulation results for the velocity of the armature, current distribution and heat distribution are presented. Furthermore, the phenomenon that current is concentrated in a single local area while heat is concentrated in a spot area and a line area is revealed. The formation mechanism of the phenomenon is proposed, which is a correction to previous literature. Finally, the influence of contact resistance and friction on the electromagnetic propulsion process is analyzed, which reveals key factors in reducing the simulation complexity of electromagnetic propulsion and helps relieve the extremely harsh environment.
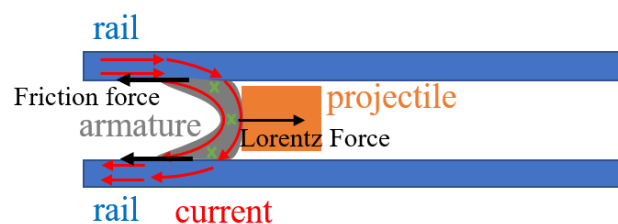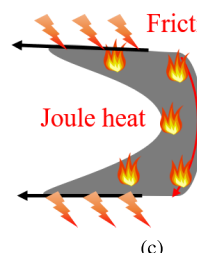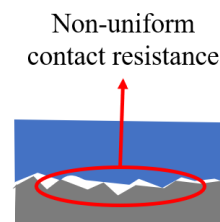

FIGURE 1. Introduction to the electromagnetic propulsion. (a) A moment of launch of a electromagnetic rail gun; (b) A schematic diagram of a typical electromagnetic propulsion system; (c) heat inside the armature; (d) contact resistance at the interface between armature and rail.

II. MULTI-FIELD PHYSICS MODEL FOR ELECTROMAGNETIC PROPULSION

Electromagnetic propulsion technology can accelerate the loaded object to an ultrahigh speed of more than 2000 m/s in milliseconds and has made breakthroughs in the fields of electromagnetic rail guns (Fig. 1a) and aircraft propulsion. A schematic diagram of a typical electromagnetic propulsion system is shown in Fig. 1b. The armature is mounted between two rails, and the object is loaded on the front of the armature. A large pulse current is applied between the two rails, creating a strong magnetic field of the order of 10 T at the armature. The armature with a high current is subjected to a large electromagnetic driving force under a strong magnetic field and thus pushes the loaded object to a high speed.
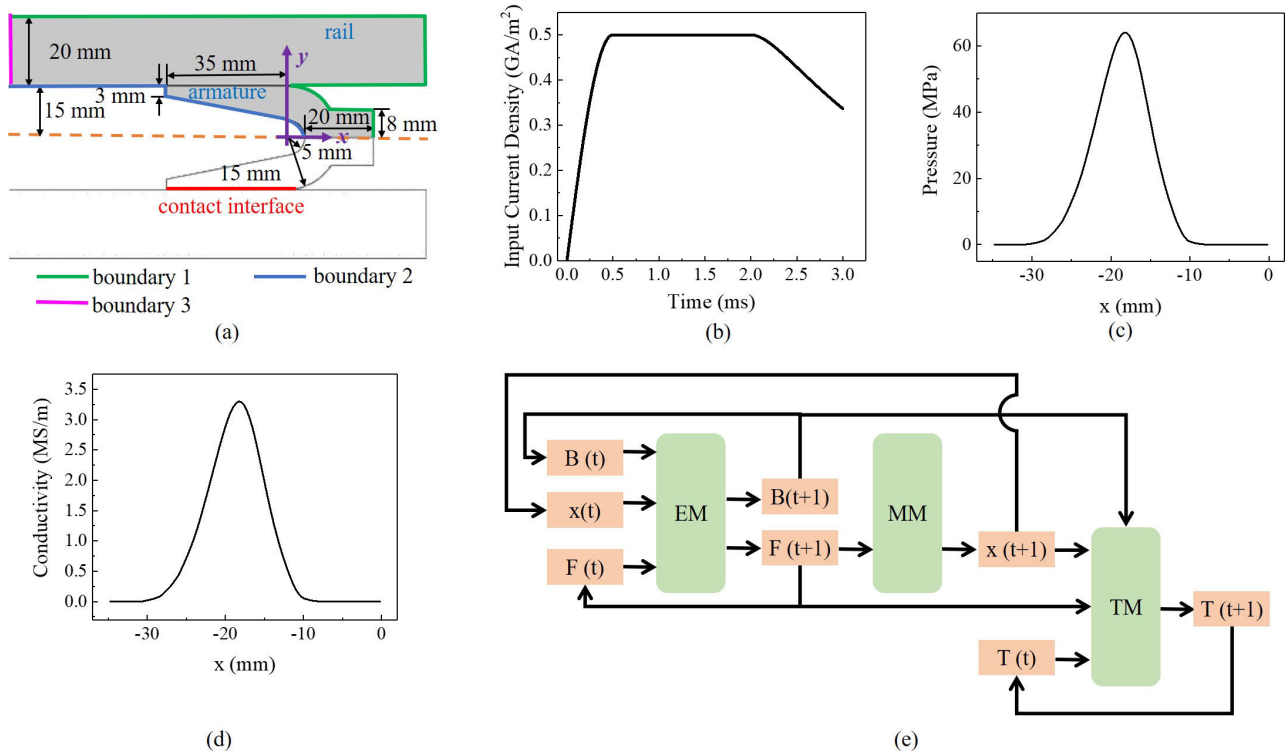
IEEE *Access*

K. Dai *et al.*: Theoretical Model and Analysis on the Locally Concentrated Current and Heat During Electromagnetic Propulsion

FIGURE 2. The simulation conditions. (a) 2-dimensional symmetric model; (b) input current density during the electromagnetic propulsion; (c) the distribution of the pressure along the contact interface caused by the armature preclamping process; (d) equivalent conductivity along the contact layer with armature preclamping; (e) multiphysics iterative process for simulation.

During the electromagnetic propulsion process, the mechanical field, the electromagnetic field, and the thermal field all undergo extremely high dynamic changes, and the multiple physical fields are coupled with each other, causing some special physical effects. For example, the change in the temperature distribution of the armature with time is simultaneously affected by the Joule heating effect and the frictional thermal effect (Fig. 1c), which are caused by the electromagnetic field and the mechanical field, respectively. As for the contact resistance between the armature and the rail (Fig. 1d), on the one hand, it is directly controlled by the pressure field distribution between the two; on the other hand, the change in the contact resistance makes the distributions of the current and magnetic field in the armature different. As a result, the electromagnetic force on the armature is affected, and the mechanical field is also changed. In other words, the electromagnetic and mechanical fields are affected by each other. Therefore, to achieve effective modeling of the multiphysics environment during electromagnetic propulsion, it is necessary to establish not only the models of each physical field but also the coupling relationship between them.

A. ELECTROMAGNETIC FIELD

The driving current of the electromagnetic propulsion system is mainly distributed in the horizontal plane. Considering the axial symmetry of the whole system, the two-dimensional

symmetric model shown in Fig. 2a is used for modeling and simulation. Based on this model, the dynamic change in the multiphysics fields of the electromagnetic propulsion system shown in Fig. 1b is studied. When there is strong pulse current (as shown in Fig. 2b) applied to the rail, the changes in the electromagnetic field of the rails and the armature can be described by the magnetic diffusion equation [18]. For the rail in Fig. 2a, the magnetic diffusion equation is

$$\frac{\partial B}{\partial t} - \frac{1}{\sigma_r \mu_r}\left(\frac{\partial^2 B}{\partial x^2} + \frac{\partial^2 B}{\partial y^2}\right) + v \cdot \frac{\partial B}{\partial x} = 0 \quad (1)$$

where B is the magnetic induction, and the positive direction is shown in Fig. 1b; t is the time; σ_r and μ_r are the conductivity and the permeability of the rail, respectively; x and y are the axes shown in Fig. 2a; and v is the actual velocity of the armature. For the sake of simplifying subsequent calculations, it is assumed that the armature is fixed and that the rails move at a high speed in the opposite direction.

To simulate the contact resistance of the contact interface between the rail and armature, a contact layer is set in the geometric model shown in Fig. 2a. To describe its piezoresistive effect, the conductivity of the contact interface is a function of pressure. Thus, σ_r in Eq. (1) can be presented as,

$$\sigma_r = \begin{cases} \sigma_{r,p}, & \text{at the contact layer} \\ \sigma_{r,0}, & \text{at the rail body} \end{cases} \quad (2)$$

K. Dai *et al.*: Theoretical Model and Analysis on the Locally Concentrated Current and Heat During Electromagnetic Propulsion

IEEE *Access*

For the armature, the velocity term in Eq. (1) will not exist, and the magnetic diffusion equation is

$$\frac{\partial B}{\partial t} - \frac{1}{\sigma_a \mu_a} \left(\frac{\partial^2 B}{\partial x^2} + \frac{\partial^2 B}{\partial y^2} \right) = 0 \qquad (3)$$

where σ_a and μ_a are the conductivity and the permeability of the armature, respectively. In fact, the rail and the armature are made of non-ferromagnetic metal, and their permeability is almost the same and is marked as μ in the following.

The boundary conditions in Eqs. (1) and (3) have been discussed in depth in a lot of literature [24], [25]. In this study, the same condition as that in the literature is taken, and then the boundary conditions for boundaries 1, 2, and 3 in Fig. 2a are,

$$B = \begin{cases} 0, & \text{boundary 1} \\ B_0, & \text{boundary 2} \\ B_0 \dfrac{H - y}{H}, & \text{boundary 3} \end{cases} \qquad (4)$$

where $B_0 = j_{in}\mu H$ is determined by the input current density j_{in}, and H is the width of the rail.

According to Ampere's law, the current density can be calculated from the magnetic induction B:

$$j_x = -\frac{1}{\mu} \frac{\partial B}{\partial y} \qquad (5)$$

$$j_y = \frac{1}{\mu} \frac{\partial B}{\partial x} \qquad (6)$$

where j_x and j_y are the current densities in the directions of x and y, respectively.

Eqs.(1) - (6) reveal the mechanism of the changes in the electromagnetic field, which is the electromagnetic model (EM) in this study.

B. MECHANICAL FIELD

The movement of the armature is driven by the electromagnetic force in the direction of x while at the same time being resisted by the friction on the interface, which can be described by Newton's second law,

$$m \frac{d^2 x_m}{dt^2} = f_{l,x} - f_r \qquad (7)$$

where m is the mass of the armature, which can be calculated by the density of aluminium in this paper; x_m is the displacement of the armature; $f_{l,x}$ is the electromagnetic force on the armature in the direction of x; and f_r is the friction force on the interface between the armature and the rail.

The friction is in direct proportion to the pressure on the interface, which is composed of the preclamping force of the armature and the electromagnetic force in the direction of y,

$$f_r = \mu_{fr}(f_n + f_{l,y}) \qquad (8)$$

where μ_{fr} is the friction coefficient of the contact interface; f_n is the pressure caused by the preclamping of the armature; and $f_{l,y}$ is the electromagnetic force on the armature in the direction of y.

To ensure good contact between the rail and the armature, the armature of the electromagnetic propulsion system is preclamped in the direction of y, which leads to a distribution of interface pressure intensity in relation to the x axis. The modeling and calculation have been discussed in [19], and

$$f_n = \int_{S_{bc}} P ds \qquad (9)$$

where P is the distribution of pressure density caused by the preclamping of the armature.

Eqs.(7) - (9) describe the dynamics of the armature movement, which is the movement model (MM) in this study.

C. THERMAL FIELD

The heat-transfer equation for solids is used to model the dynamic changes in the thermal field inside the rail body and the armature body:

$$\rho C_p \frac{\partial T}{\partial t} = k \left(\frac{\partial^2 T}{\partial x^2} + \frac{\partial^2 T}{\partial y^2} \right) + Q + q_0 \qquad (10)$$

where ρ, C_p and k are the density, the specific heat, and the thermal conductivity of the solid object, respectively; T is the temperature; Q is the power density of the heat source; and q_0 is the heat flow at the boundary.

For the heat source Q in Eq. (10), consider Joule heating inside the rail and the armature and frictional heating on the contact interface,

$$Q = \begin{cases} Q_a, & \text{rail body and armature body} \\ Q_s, & \text{contact interface} \end{cases} \qquad (11)$$

For the surface of the armature and the rail exposed to the air, considering the heat dissipation effect caused by air heat convection,

$$q_0 = h(T_{ext} - T) \qquad (12)$$

where h is the heat transfer coefficient of air and T_{ext} is the temperature of the air.

Eqs. (10) - (12) describe the dynamic changes in the temperature inside the rail and the armature, which is the thermal model (TM) in this study.

D. COUPLING RELATIONSHIP OF THE MULTI-FIELDS

As analyzed above, the coupling effect of the multiphysics fields is the source of some special effects, which have an important influence on the extreme environment during electromagnetic propulsion. The modeling of the coupled electromagnetic field, mechanical field and thermal field in this study is as follows.

In the mechanical field, the electromagnetic force is essentially the Lorentz force and is determined by the current density and the magnetic induction of the electromagnetic field,

$$f_{l,x} = -\int_{S_a} B j_y ds \qquad (13)$$

IEEE *Access*

K. Dai *et al.*: Theoretical Model and Analysis on the Locally Concentrated Current and Heat During Electromagnetic Propulsion

$$f_{l,y} = \int_{S_a} B j_x \, ds \tag{14}$$

In Eq. (1) for the model of the electromagnetic field, the velocity v is determined by the movement of the armature,

$$v = \frac{dx_m}{dt} \tag{15}$$

In Eq. (2) for the model of the electromagnetic field, $\sigma_{r,p}$ describes the contact resistance influenced by the pressure density, which is determined by the Cooper-Mikic-Yovanovich correlation [26]:

$$\sigma_{r,p} = 1.25 \frac{2}{\frac{1}{\sigma_r} + \frac{1}{\sigma_a}} \frac{m_{asp}}{\sigma_{asp}} \left(\frac{P + f_{l,y}/S_{bc}}{H_c} \right)^{0.95} d_{bc} \tag{16}$$

where m_{asp} and σ_{asp} are the average slope and average height of the asperities at the contact interface, respectively; H_c is the microhardness; and d_{bc} is the thickness of the contact layer in Fig. 2a.

In Eq. (11) for the model of the thermal field, the Joule heat is determined by the current density and the conductivity in the model of the electromagnetic field,

$$Q_a = \begin{cases} \left(j_x^2 + j_y^2 \right)/\sigma_r, & \text{rail} \\ \left(j_x^2 + j_y^2 \right)/\sigma_a, & \text{armature} \end{cases} \tag{17}$$

The friction heat is determined by the friction force and the velocity in the model of the mechanical field, and the friction force is influenced by the electromagnetic force:

$$Q_s = \mu_{fr} \left(P + \frac{f_{l,y}}{S_{bc}} \right) v \tag{18}$$

where S_{bc} is the contact area between the rail and the armature.

Eqs. (1) - (18) above have built a whole model of the coupled multiphysics fields, forming the basis for the following simulations and analysis.

III. SIMULATION
A. SIMULATION METHOD

Based on the proposed dynamic model, multifield simulation of the electromagnetic propulsion process is realized via COMSOL software. The geometry and dimensional parameters of the rail and armature are shown in Fig. 2a. A two-dimensional symmetric model is used to reduce the computational complexity. The input current of the electromagnetic propulsion system is shown in Fig. 2b according to a practical system, which first increases to approximately 0.5 GJ/m^2 within about 0.5 ms, then maintains this maximum current density for about 1.5 ms, and finally decreases slowly in the last 1 ms. The preclamping process of the armature adopts the same setting as that in the literature [18], [19], and it has the maximum contact pressure and minimum contact resistance in the middle of the contact interface of the rail and the armature, as shown in Fig. 2c and Fig. 2d. The calculation

TABLE 1. Parameters in simulation.

Parameter	Value
$\sigma_{r,0}$	1.40×10^7 S/m
μ	$4\pi \times 10^{-7}$ H/m
σ_a	2.50×10^7 S/m
μ_{fr}	0.02
ρ in the rail	8900 kg/m^3
ρ in the armature	2700 kg/m^3
C_p in the rail	386 J/kg/K
C_p in the armature	880 J/kg/K
k in the rail	397 W/m/K
k in the armature	237 W/m/K
h	10 W/(m$^2\cdot$K)
T_{ext}	293.15 K
m_{asp}	0.4
σ_{asp}	1 μm
H_c	1 GPa
d_{bc}	5 μm

flow of the simulation is shown in Fig. 2e. The electromagnetic propulsion process is sequentially divided into a large number of time pieces of microseconds. In a single time piece, the quasistatic electromagnetic model is first used to calculate the dynamic change in the electromagnetic field, and then the results are introduced into the mechanical model to update the velocity and displacement. Finally, the results of the electromagnetic model and the mechanical model are introduced into the thermal model to update the temperature distribution. The last-moment solution of the previous time piece is taken as the initial value of the following time piece, and this iteration is carried out to realize the simulation of the whole electromagnetic propulsion process. The values of all the parameters in the simulation are listed in Table 1.

B. DISPLACEMENT AND VELOCITY: UP TO 1800 M/S WITHIN MILLISECONDS

The simulation results of the armature movement are shown in Fig. 3. The armature is gradually moving and accelerating under the electromagnetic force. The calculation accuracy is enough to simulate the millimeter-scale or even finer motion in the early propulsion process (Fig. 3a). For the whole propulsion process, the armature is accelerated to nearly 1800 m/s in just 3 ms, with the propulsion distance of only 2.57 m (Fig. 3b). These results fully demonstrate the possibility of advanced weapons with small volume, high emission frequency, and ultrahigh kinetic energy via electromagnetic propulsion. However, with such a strong acceleration capability, the armature and its propelled objects withstand up to $6.26 \times 10^4 \, g$ of inertial force in this process, posing a serious challenge to the reliability of the electronic components inside the propulsion object.

K. Dai et al.: Theoretical Model and Analysis on the Locally Concentrated Current and Heat During Electromagnetic Propulsion
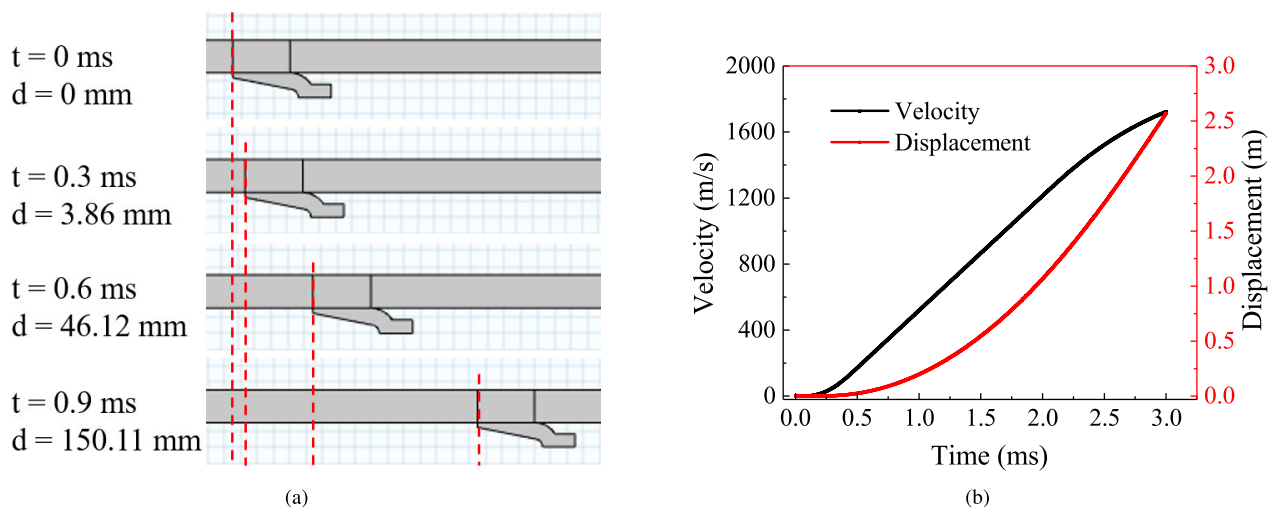
IEEE Access

(a)

(b)

FIGURE 3. The simulation of the armature movement. (a) The accelerated movement process of the armature; (b) the relationships among velocity, displacement and time during electromagnetic propulsion.
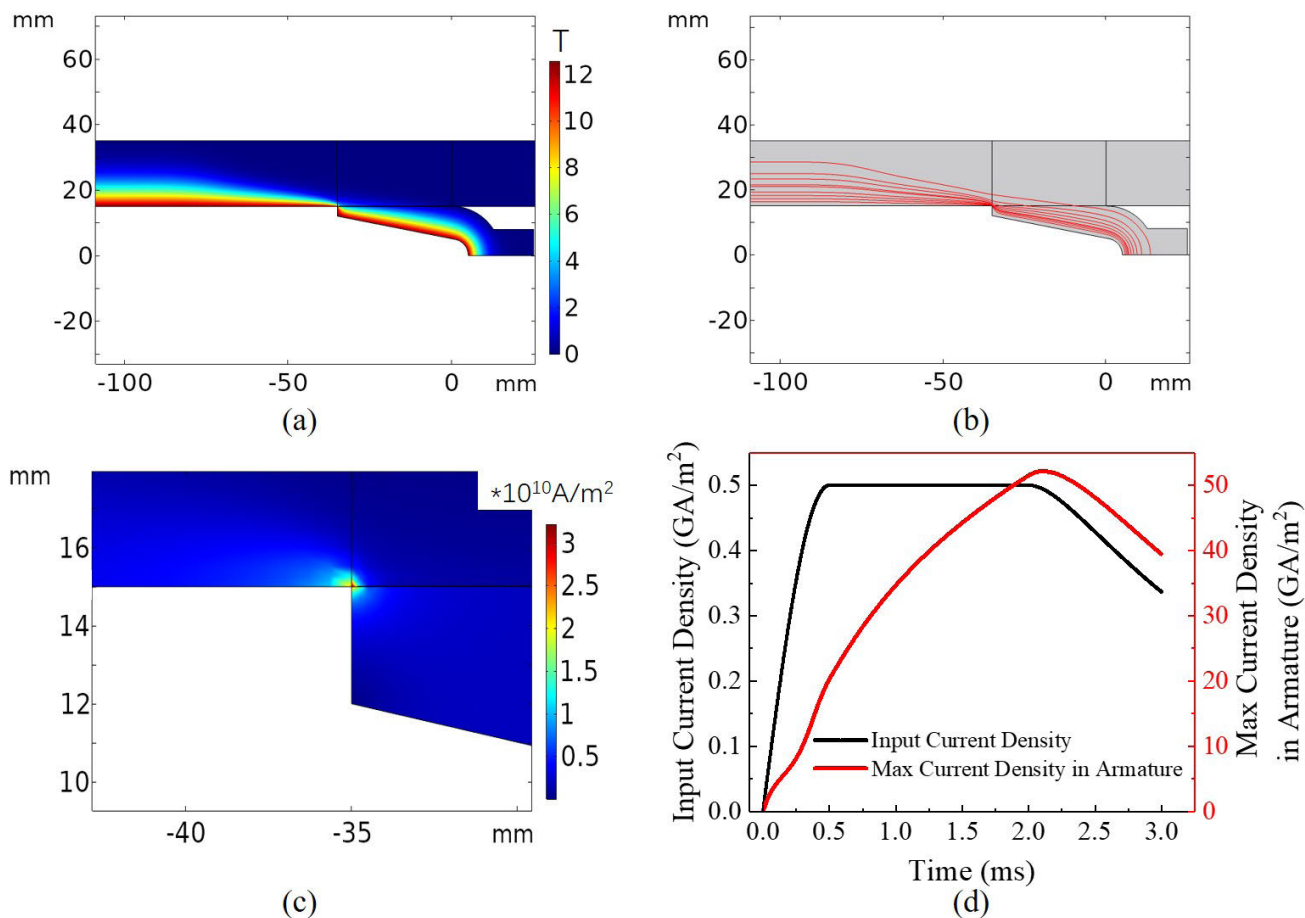

(a)

(b)

(c)

(d)

FIGURE 4. Simulation of the electromagnetic field and current distribution. (a) Magnetic induction ($t = 0.6$ ms); (b) current line distribution ($t = 0.6$ ms); (c) current density distribution ($t = 0.6$ ms); (d) the relationships among the maximum current density in the armature, input current density and time.

C. CURRENT DISTRIBUTION: CONCENTRATION IN A SINGLE LOCAL AREA

Figs. 4a-c shows the simulation results of the electromagnetic field (taking $t = 0.6$ ms as an example). According to Fig. 4a,

from the inner surface of the rail to the outer, the magnetic induction intensity first decays rapidly to a relatively low level along the perpendicular direction to the surface and then decays slowly to zero.

IEEE Access

K. Dai et al.: Theoretical Model and Analysis on the Locally Concentrated Current and Heat During Electromagnetic Propulsion

Based on the electromagnetic distribution, the current density in the rail and armature is calculated via Eqs. (5) and (6), as shown in Figs. 4b-c. Obviously, in the rail, the current distribution has a skin effect and is densely distributed in the area close to the inner surface of the rail, which is at a level of GA/m^2. The current inside the armature also has a certain degree of skin effect, but it is less conspicuous than the rail. These effects are consistent with the conclusions in previous literature [18]. As shown in Fig. 4c, the maximum current density appears at the left vertex of the interface between rail and armature, with a value of several tens of GA/m^2. It is worth noting that there is only one current concentration area in the rail and armature, which is inconsistent with the results in previous literature [18]: they claim that there is a second current concentration area at the middle of the contact interface between the rail and the armature, which is the maximum pressure point in Fig. 2c, due to the contact resistance's piezoresistive effect. The mechanism of the newly discovered phenomenon is further discussed in Section IV-A.

Fig. 4d further shows the relationship between the maximum current density and time. It is worth noting that the trend of maximum current density is not exactly the same as that of the input current density. When the input current density is approximately linearly increasing, the maximum current density increases faster than a linear relationship. When the input current density is approximately constant, the maximum current density is still rising at an increasingly slower speed. This phenomenon is also due to the velocity skin effect. As the armature speed increases, a greater proportion of the current concentrates near the surface area of the rail and armature, and a larger maximum current density appears when the input current density is constant.

D. HEAT DISTRIBUTION: A HOT SPOT AND A HOT LINE

Fig. 5a shows the temperature distribution inside the rail and the armature (also in the case of $t = 0.6$ ms). The temperature distribution is concentrated on the contact interface of the rail and armature (a hot line), as well as the upper-left vertex of the armature (a hot spot). Even if electromagnetic propulsion is carried out only 20% of the total time at this time point, the maximum temperature of the hot spot has increased by nearly 391.5 K, and the average temperature of the hot line has increased by more than 120 K compared with the ambient temperature.

Fig. 5b further shows the relationship of the maximum temperature of the hot spot (T_1) and the average temperature of the hot line (T_2) over time. Before the input current decreases, T_1 and T_2 are continuously rising, but when the input current begins to fall, T_1 and T_2 decrease. Throughout the whole process, the maximum temperature increase of T_1 is close to 1885 K, and that of T_2 is more than 260 K (this paper mainly studies the factors affecting the temperature increase and ignores the change in physical state). Such a high temperature can cause the softening of the rail and the armature at the contact interface. Coupled with the extreme frictional force
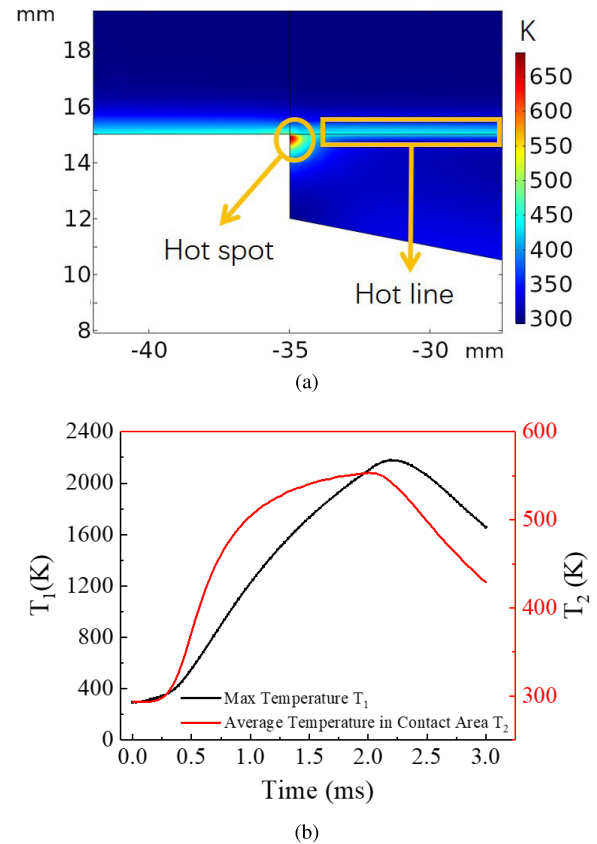

(a)

(b)

FIGURE 5. Simulation of the temperature distribution. (a) Temperature distribution characteristics with hot spots and hot lines ($t = 0.6$ ms); (b) Relationships between the maximum temperature in the armature (T_1), average temperature on the contact interface (T_2) and time.

and pressure, the softening can further cause erosion, which damages the surface of the rail and the armature.

IV. DISCUSSION

A. THE ESSENCE OF CURRENT CONCENTRATION: SKIN EFFECT EXCEEDS PIEZORESISTIVE EFFECT

The results of the single current concentration area shown in Fig. 4c seem to contradict the reports of two separate current concentration areas in the literature [18]. In fact, the disappearance of the second current concentration region (located in the middle of the contact interface) is due to the coupling of the current skin effect and the contact resistance's piezoresistive effect. Actually, the results of the dual current concentration area in the previous literature [18] take into consideration the contact resistance's piezoresistive effect but ignore the current skin effect.

The schematic diagram of the current path under such an assumption is shown in Fig. 6a. Due to the preclamping process of the armature, the pressure in the middle of the contact interface is much larger than that at the left vertex. Correspondingly, the contact resistance at the left vertex of the contact interface is much larger than that in the middle. For an intuitive comparison, the unevenly distributed contact
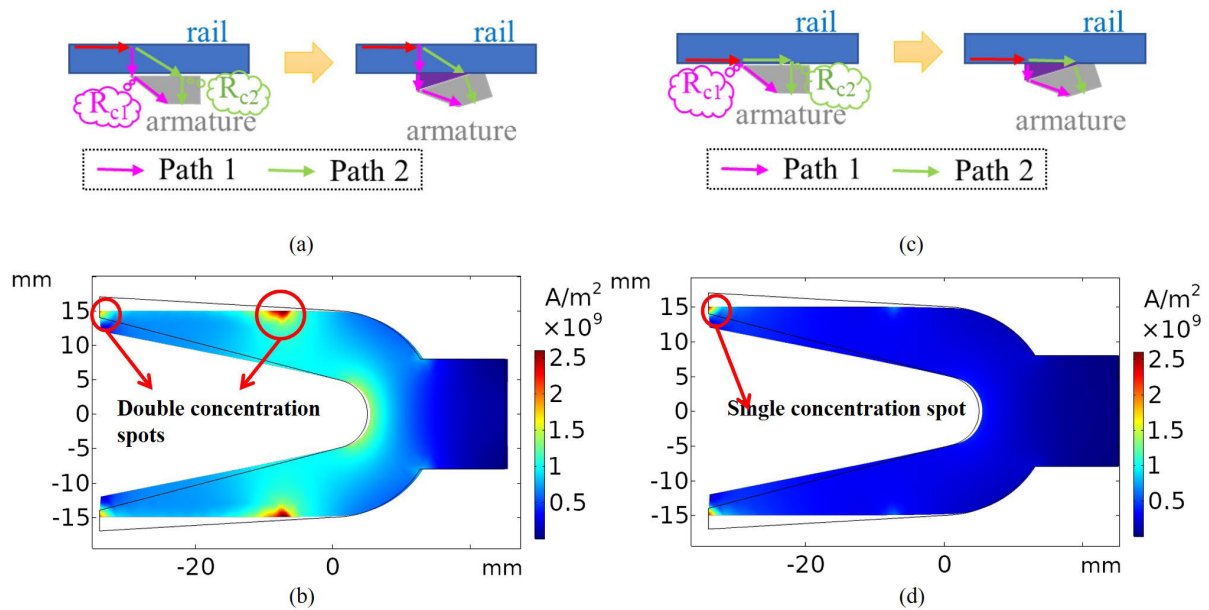
K. Dai *et al.*: Theoretical Model and Analysis on the Locally Concentrated Current and Heat During Electromagnetic Propulsion

IEEE *Access*

FIGURE 6. Coupling of current skin effect and the contact resistance's piezoresistive effect. (a) Current path analysis for non-skin current; (b) Double concentration spots of the current density under non-skin current; (c) Current path analysis for skin current; (d) Single concentration spots of the current density under skin current.

resistance in Fig. 6a is equivalent to a uniform resistivity layer with unequal thickness, sandwiched between the rail and the armature. It is obvious that current path 2 (passing through the middle of the contact interface) is likely to have a lower cumulative resistance than current path 1 (passing through the left end of the contact interface), which is the explanation for the double current concentration areas in the literature [18]. Fig. 6b shows the simulation results under this assumption via the model in the literature [18], which is consistent with the analysis in Fig. 6a.

However, considering the coupling of the current skin effect and the contact resistance's piezoresistive effect in practical systems, the situation becomes completely different. A schematic diagram of the current path under such a more realistic assumption is shown in Fig. 6c. Even with the consideration of the nonuniform thickness layer equivalent to the contact resistance, the cumulative resistance of current path 1 (passing through the left vertex of the contact interface) is still significantly smaller than that of current path 2 (passing through the middle of the contact interface), revealing the physical mechanism of the single current concentration area shown in Fig. 4c, which is more consistent with the practical electromagnetic propulsion system.

As analyzed above, the main drawback of the model in the literature [18] is that the current skin effect is not considered. The critical importance of this defect is demonstrated through comparative simulation: by compulsively setting the input current as the skin current, the defect of the literature model is equally compensated, although it is still far from the actual situation simulated by the proposed model in this paper. Under such a correction, the current density distribution concentrates in one single area (Fig. 6d), which

is consistent with the simulation results of the multiphysics coupling model studied in this paper (Fig. 4c). This result fully demonstrates that the coupling of the current skin effect and the contact resistance's piezoresistive effect is the essential mechanism of the single current concentration area in the armature.

In fact, the current skin effect is always significant throughout the whole process of electromagnetic propulsion and cannot be ignored. In the early stage of electromagnetic propulsion, the input current is continuously rising sharply, so the current signal has significant high-frequency components, resulting in a current skin effect dominated by the high-frequency current, as shown in Fig. 7a. The current at this stage is characterized by a nearly uniform skin depth along the direction of the rail, consistent with the skin effect dominated by high-frequency currents. When the input current enters the platform stage in Fig. 2b, its high-frequency component almost disappears. However, during this time period, the armature already has non-negligible velocity, resulting in a current skin effect dominated by high speed. Fig. 7b shows the current skin effect during this period. Along the rail, the current has smaller skin depth where it is closer to the armature, which is consistent with the general rule of the skin effect dominated by high speed and provides an explanation for the position of the current concentration area in Fig. 4c. For the above two reasons, the current skin effect exists throughout the whole process of electromagnetic propulsion. Fig. 7c shows the current skin depth change during the whole process. The current skin depth is defined where the total current inside it is 90% of the total current of the cross-section of the rail. Obviously, the current skin depth is always significantly smaller than the width of the rail.
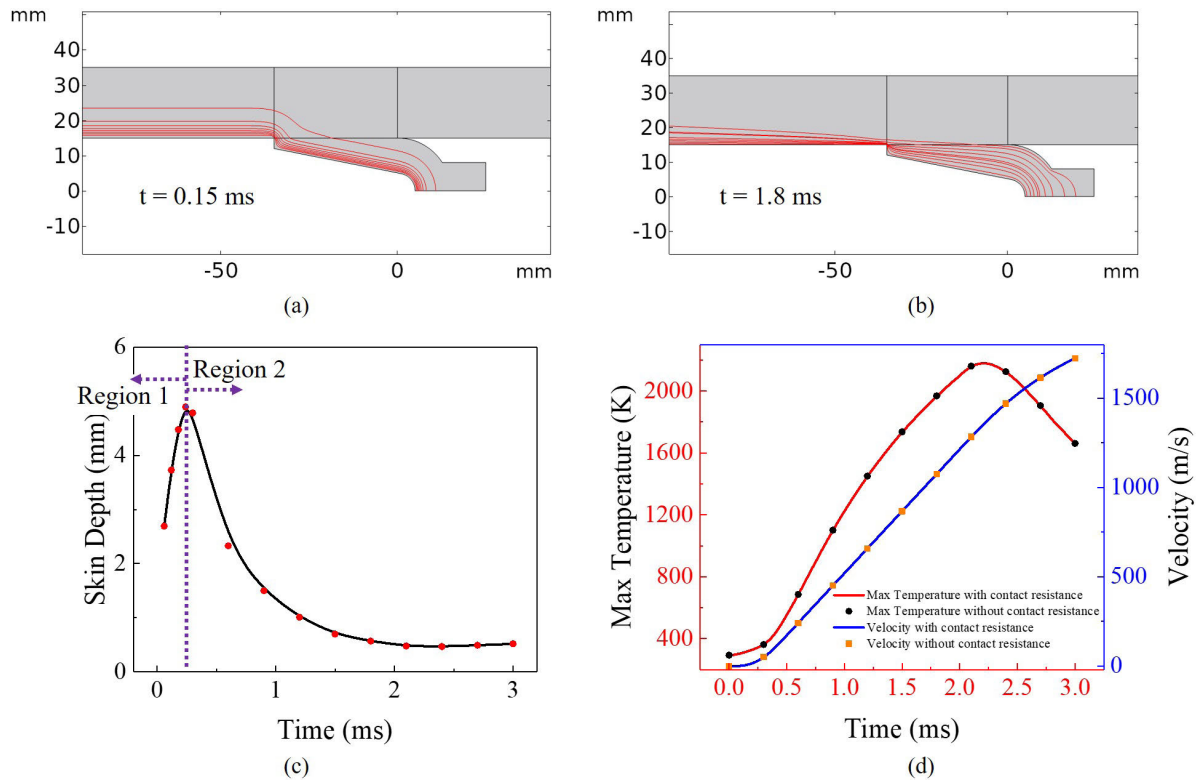
IEEE *Access*

K. Dai *et al.*: Theoretical Model and Analysis on the Locally Concentrated Current and Heat During Electromagnetic Propulsion

FIGURE 7. Further analysis of current skin effect and the contact resistance's piezoresistive effect. (a) The current skin effect dominated by high frequency current in the early stage of electromagnetic propulsion; (b) Current skin effect dominated by high speed in the later stage of electromagnetic propulsion; (c) The relationship between skin depth and time; (d) The maximum temperature and velocity of the armature with and without consideration of the contact resistance's piezoresistive effect.

Therefore, the influence of the current skin effect on the electromagnetic field and current distribution should undoubtedly not be neglected.

Based on the above analysis, the influence of the contact resistance's piezoresistive effect on the current distribution is actually offset by the current skin effect. The current still enters the armature mainly through the left vertex of the contact interface and leads to the single current concentrated area at this position, which is hardly affected by the contact resistance distribution of other parts on the contact interface. This conclusion implies that the simulation of the electromagnetic propulsion process may neglect the influence of contact resistance without significant accuracy loss. Fig. 7d shows the simulated results of the speed and maximum temperature during the electromagnetic propulsion process while considering or ignoring the contact resistance. Obviously, the simulation results of the two are almost completely coincident. Therefore, a simple model that ignores the contact resistance can effectively reduce the computational complexity of electromagnetic propulsion simulations.

B. THE ESSENCE OF HEAT CONCENTRATION: THE CONTRIBUTION OF FRICTIONAL HEAT IS NOT NEGLIGIBLE

The electromagnetic propulsion simulations in some previous literature only consider the contribution of Joule heat, while frictional heat is neglected or overly idealized. However, according to the "hot line" result at the contact interface of the rail and the armature, as shown in Fig. 5c, the frictional heat may have a non-negligible contribution. In order to investigate this problem in depth, Fig. 8a presents the frictional thermal power distribution on the contact interface at different times. During the electromagnetic propulsion process, even though the coefficient of friction is only 0.02, the frictional thermal power on the entire contact interface is on the order of tens of GJ/m^2. It is noteworthy that the maximum frictional thermal power is at the middle of the contact interface (which is also the maximum pressure point in Fig. 2c), with a super high value of more than one hundred GJ/m^2, as shown in Fig. 8b. Such high thermal friction power density is caused by high pressure on the order of MPa and high speed on the order of km/s.

To further analyze the influence of frictional heat on the temperature distribution in the armature, the total frictional heat power and total Joule heat power during electromagnetic propulsion are presented in Fig. 8c. As time goes by, the speed of the armature increases, and the ratio of frictional heat power to Joule heat power also increases. Friction becomes the main heat source of the armature. Therefore, the influence of frictional heat on the heat distribution of the armature is not negligible. For comparison, simulation results that ignore the frictional heat are shown in Fig. 8d (still taking
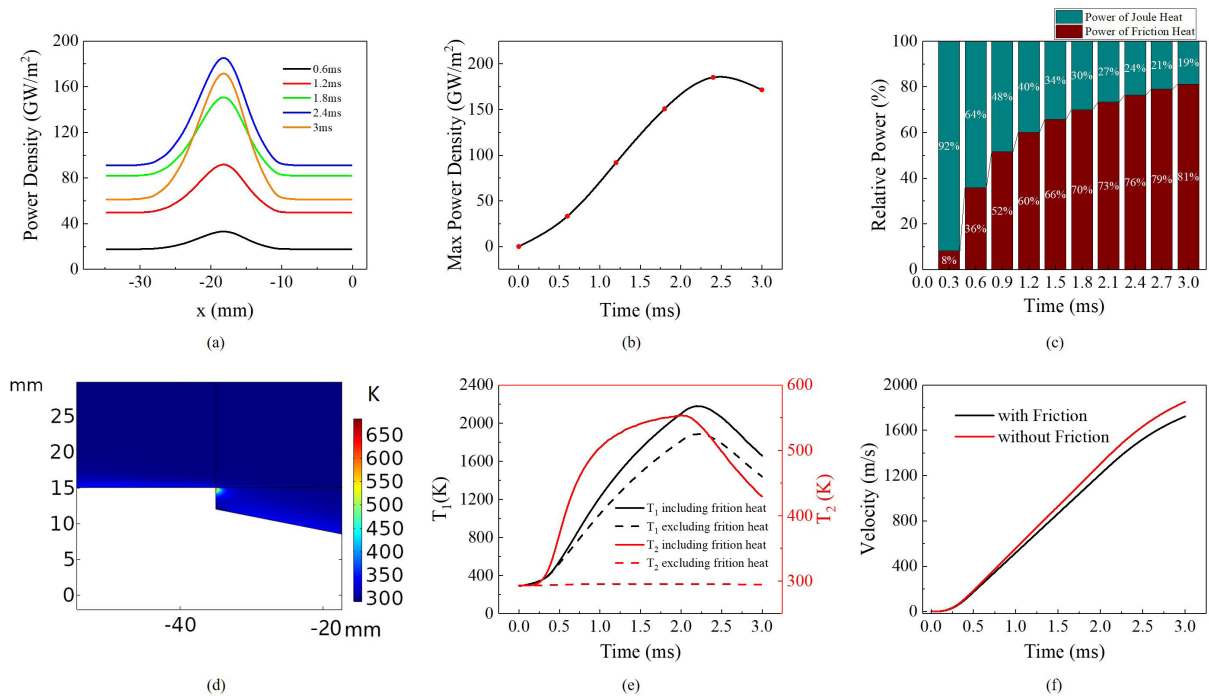
K. Dai *et al.*: Theoretical Model and Analysis on the Locally Concentrated Current and Heat During Electromagnetic Propulsion

IEEE *Access*

FIGURE 8. Analysis of the influence of friction on electromagnetic propulsion. (a) Frictional thermal power distribution at the contact interface between the rail and the armature; (b) the maximum power density of the friction heat along the contact interface; (c) the relative power ratio between the friction heat and the Joule heat during the electromagnetic propulsion process; (d) temperature distribution without considering the frictional heat effect; (e) simulation of the maximum temperature T_1 in the armature and the average temperature T_2 on the contact interface while including and excluding the friction heat; (f) the relationship between velocity and time with and without considering the friction force.

$t = 0.6$ ms as an example). Compared with the simulation results considering the frictional heat (Fig. 5c), not only does the distribution of the hot line disappear completely, but the area range of the hot spot is also significantly reduced, and the maximum temperature is lowered. Furthermore, Fig. 8e shows the variation in the maximum temperature T_1 in the armature and the average temperature T_2 on the contact interface during electromagnetic propulsion without considering the frictional heat. Compared with the simulation results considering the frictional heat, not only does the temperature rise of T_2 during the whole process almost completely disappear, but the maximum value of T_1 is also reduced by more than 13%. Therefore, further reduction in the friction coefficient is the key to relieving the extreme environment. In addition, the simulation that ignores the friction force also causes a 7.52% increase in the final speed after electromagnetic propulsion compared with the actual situation, as shown in Fig. 8f. These simulation results fully demonstrate that the influence of friction on the electromagnetic propulsion process is not negligible, even with a small friction coefficient.

V. CONCLUSION

In summary, in this paper, a unified multifield coupling model for the dynamic changes in the mechanical field, electromagnetic field and thermal field during electromagnetic propulsion is constructed, and some key coupling relationships are proposed. Through this model, an effective dynamic

simulation of the armature acceleration process and the current and temperature distribution in the rail and armature during electromagnetic propulsion is realized. The simulation results show that the armature can be accelerated to an ultrahigh speed of nearly 1800 m/s within 3 ms. The influence of the contact resistance's piezoresistive effect as well as the friction effect at the armature–rail contact interface on the electromagnetic propulsion process is discussed in depth. For the contact resistance, this paper corrects the conclusions in previous literature through simulation and theoretical analysis. The current in the rail enters the armature mainly from the left vertex of the contact interface due to the current skin effect and forms a single concentration area, which is hardly influenced by the distribution of contact resistance on the armature–rail contact interface. A simplified model that ignores the contact resistance's piezoresistive effect can achieve almost the same simulation results of armature speed, current distribution, and temperature distribution as the original model, and can reduce the computational complexity at the same time. For friction, this paper quantitatively analyzes the relative power ratio of frictional heat and Joule heat inside the armature with a friction coefficient of 0.02, revealing that friction heat has a greater power contribution than Joule heat during the high-speed movement of the armature. The simulation results show that the friction effect has a considerable influence on the maximum temperature and movement speed of the armature. Specifically, friction is the key factor in the

overall temperature of the armature–rail contact interface. Therefore, further reducing the friction coefficient of the contact interface is still the key to effectively reducing the contact interface temperature, relieving the extreme environment of the propulsion process, and avoiding irreversible damage such as erosion. In sum, the theoretical analysis in this paper provides the foundation for simulation of multiphysics fields with low computational complexity and highlights a feasible path for relieving the extreme environment during electromagnetic propulsion, which will greatly promote the practical application of electromagnetic propulsion technology.

REFERENCES

[1] H. D. Fair, "Advances in electromagnetic launch science and technology and its applications," *IEEE Trans. Magn.*, vol. 45, no. 1, pp. 225–230, Jan. 2009.

[2] A. Musolino, R. Rizzo, and E. Tripodi, "The double-sided tubular linear induction motor and its possible use in the electromagnetic aircraft launch system," *IEEE Trans. Plasma Sci.*, vol. 41, no. 5, pp. 1193–1200, May 2013.

[3] J. T. Tzeng, "Structural mechanics for electromagnetic rail guns," in *Proc. 12th Symp. Electromagn. Launch Technol.*, May 2004, pp. 127–132.

[4] T. Siaenen, M. G. Schneider, and M. J. Loffler, "Rail gun muzzle velocity control with high accuracy," *IEEE Trans. Plasma Sci.*, vol. 39, no. 1, pp. 133–137, Jan. 2011.

[5] W. Ma and J. Lu, "Thinking and study of electromagnetic launch technology," *IEEE Trans. Plasma Sci.*, vol. 45, no. 7, pp. 1071–1077, Jul. 2017.

[6] W. Ma, J. Lu, and Y. Liu, "Research progress of electromagnetic launch technology," *IEEE Trans. Plasma Sci.*, vol. 47, no. 5, pp. 2197–2205, May 2019.

[7] J. Li, S. Li, P. Liu, Y. Gui, N. Su, J. Dong, J. Zhang, Y. Gao, W. Yuan, and P. Yan, "Design and testing of a 10-MJ electromagnetic launch facility," *IEEE Trans. Plasma Sci.*, vol. 39, no. 4, pp. 1187–1191, Apr. 2011.

[8] H. Zhang, K. Dai, and Q. Yin, "Ammunition reliability against the harsh environments during the launch of an electromagnetic gun: A review," *IEEE Access*, vol. 7, pp. 45322–45339, 2019.

[9] W. Zhi-Heng, W. Min, and L. Xiao-Jiang, "Numerical modeling of electromagnetic railgun rail temperature field," *Int. J. Appl. Electromagn. Mech.*, vol. 51, no. 2, pp. 173–183, Jun. 2016.

[10] S. A. Taher, M. Jafari, and M. Pakdel, "A new approach for modeling electromagnetic railguns," *IEEE Trans. Plasma Sci.*, vol. 43, no. 5, pp. 1733–1741, May 2015.

[11] Y.-H. Lee, S.-H. Kim, B.-H. Lee, S. An, and K.-S. Yang, "Experimental tests of a 25 mm square-bore railgun," in *Proc. IEEE 16th Int. Symp. Electromagn. Launch Technol.*, May 2012, pp. 1–6.

[12] Y. He, Y. Guan, G. Gao, Y. Li, X. Qiu, B. Wei, and S. Song, "Efficiency analysis of an electromagnetic railgun with a full circuit model," *IEEE Trans. Plasma Sci.*, vol. 38, no. 12, pp. 3425–3428, Dec. 2010.

[13] B. Tang, Q. Lin, and B. Li, "Research on thermal stress by current skin effect in a railgun," *IEEE Trans. Plasma Sci.*, vol. 45, no. 7, pp. 1689–1694, Jul. 2017.

[14] B. Tang, Y. Xu, Q. Lin, and B. Li, "Synergy of melt-wave and electromagnetic force on the transition mechanism in electromagnetic launch," *IEEE Trans. Plasma Sci.*, vol. 45, no. 7, pp. 1361–1367, Jul. 2017.

[15] B.-M. Li and Q.-H. Lin, "Analysis and discussion on launching mechanism and tactical electromagnetic railgun technology," *Defence Technol.*, vol. 14, no. 5, pp. 484–495, 2018.

[16] M. Ghassemi and R. Pasandeh, "Thermal and electromagnetic analysis of an electromagnetic launcher," *IEEE Trans. Magn.*, vol. 39, no. 3, pp. 1819–1822, May 2003.

[17] M. S. Bayati, A. Keshtkar, and A. Keshtkar, "Thermal computation in railgun by hybrid time domain technique 3-D-FEM-IEM," *IEEE Trans. Plasma Sci.*, vol. 39, no. 1, pp. 18–21, Sep. 2010.

[18] Q. Yin, H. Zhang, H.-J. Li, and Y.-X. Yang, "Analysis of in-bore magnetic field in C-shaped armature railguns," *Defence Technol.*, vol. 15, pp. 83–88, Feb. 2019.

[19] S. Xia, J. He, L. Chen, Z. Xiao, and J. Li, "Studies on interference fit between armature and rails in railguns," *IEEE Trans. Plasma Sci.*, vol. 39, no. 1, pp. 186–191, Jan. 2011.

[20] F. Gong, "Study of erosion mechanism at the armature-rail contact interface in railgun," Ph.D. dissertation, Nanjing Univ. Sci. Technol., Nanjing, China, 2014.

[21] D. Ren, X. Feng, L. Lu, M. Ouyang, S. Zheng, J. Li, and X. He, "An electrochemical-thermal coupled overcharge-to-thermal-runaway model for lithium ion battery," *J. Power Sources*, vol. 364, pp. 328–340, Oct. 2017.

[22] D. Ren, X. Feng, L. Lu, X. He, and M. Ouyang, "Overcharge behaviors and failure mechanism of lithium-ion batteries under different test conditions," *Appl. Energy*, vol. 250, pp. 323–332, Sep. 2019.

[23] D. Ren, X. Liu, X. Feng, L. Lu, M. Ouyang, J. Li, and X. He, "Model-based thermal runaway prediction of lithium-ion batteries from kinetics analysis of cell components," *Appl. Energy*, vol. 228, pp. 633–644, Oct. 2018.

[24] J. D. Powell, D. J. Walbert, and A. E. Zielinski, "Two-dimensional model for current and heat transport in solid-armature railguns," Army Res. Lab., Adelphi, MD, USA, Tech. Rep. ARL-TR-74, 1993.

[25] X. Li and C. Weng, "Three-dimensional investigation of velocity skin effect in U-shaped solid armature," *Prog. Natural Sci.*, vol. 18, no. 12, pp. 1565–1569, 2008.

[26] M. M. Yovanovich, "Four decades of research on thermal contact, gap, and joint resistance in microelectronics," *IEEE Trans. Compon. Packag. Technol.*, vol. 28, no. 2, pp. 182–206, Jun. 2005.

KEREN DAI received the B.E. and Ph.D. degrees from Tsinghua University, Beijing, China, in 2014 and 2018, respectively. He is currently an Assistant Professor with the School of Mechanical Engineering, Nanjing University of Science and Technology. His research interests include system modeling and simulation, signal processing, power management systems, and micro power devices.

YUXIN YANG was born in Jiangsu, China. He is currently pursuing the Ph.D. degree with the ZNDY of Ministerial Key Laboratory, Nanjing University of Science and Technology. His current research interests include electromagnetic interference technology, electromagnetic shielding technology, and intelligent ammunition fuze technology.

QIANG YIN was born in Jiangxi, China. He is currently pursuing the Ph.D. degree with the Ministerial Key Laboratory of ZNDY, Nanjing University of Science and Technology. His current research interests include electromagnetic launch technology and intelligent ammunition fuze technology.

HE ZHANG was born in Henan, China. He received the Ph.D. degree in measurement technology and instruments from the Nanjing University of Aeronautics and Astronautics, Nanjing, China.

He is currently a Professor with the School of Mechanical Engineering, Nanjing University of Science and Technology, Nanjing. His research interests include mechatronics and weapon system applications. Prof. Zhang is the Director of the Institute of Mechanical and Electrical Engineering, NJUST, the Associate Director of the ZNDY National Defense Key Laboratory, and the Editorial Board of the *Journal of Detection & Control*.